Journal of Electrical Engineering, Vol. 74, No. 5, 2023, pp. 344-356

sciendo

PAPERS

Model-free predictive current control of Syn-RM based on time delay estimation approach

Mohamed Essalih Boussouar[1, 4], Abdelghani Chelihi[2, 3], Khaled Yahia[4, 5], Antonio J. Marques Cardoso [4]

This paper investigates an optimal model-free control design for a synchronous reluctance motor (Syn-RM) with unknown nonlinear dynamic functions, parameter variations, and disturbances. The idea is to combine a predictive control with a time-delay estimation technique (TDE) in order to successfully deal with the system's uncertainties and make the Syn-RM control scheme easy to implement in real-time. This model-free control strategy comprises two cascade control loops namely outer and inner loops. The outer loop is designed for the mechanical part of Syn-RM to ensure the convergence of the speed dynamics by using a proportional-integral controller while the inner loop is developed to control the uncertain dynamics of currents via an optimal robust controller. In the proposed current loop, the predictive control is enhanced by the inclusion of ultra-local model theory where dynamic functions and disturbances are estimated by instantaneous input-output measurements of the Syn-RM using the TDE approach. Moreover, a particle swarm optimization (PSO) algorithm is also proposed to find the optimal design parameters to improve the dynamic performances of the closed-loop control system. Numerical validation tests of the proposed TDE-based model-free predictive current control (TDE-MFPCC) method are performed in the simulation environment of the Syn-RM system, and the results show the robustness and the effectiveness of the proposed TDE-MFPCC compared to the conventional model-based PCC.

Keywords: synchronous reluctance motor (Syn-RM), model-free control, predictive current control, time-delay estimation.

1 Introduction

The synchronous reluctance motor (Syn-RM) is an alternating current motor that operates on the principle of reluctance torque, as opposed to conventional induction motors that rely on the principle of rotor current induction to generate torque [1]. Syn-RM uses the magnetic reluctance of the rotor to generate torque resulting in increased efficiency, power factor, and dynamic performance [2, 3]. The Syn-RM machine also has a higher starting torque than the traditional induction motor making it excellent for applications requiring high starting torque [4]. Recent advancements in rotor design and high-complexity embedded systems have made this motor an attractive option for various applications [5]. In addition, its sturdy design is further enhanced by a wingless and magnetless rotor.

The promising potential of the control engineering of Syn-RM machines has led to the attraction of many researchers to this field of study. Field-oriented control (FOC) is a widely used technique for regulating the torque and flux of a Syn-RM [6, 7]. By utilizing stator current vectors, FOC allows for precise control of the motor's performance. There are two modes in which FOC can be implemented. The first is direct field-oriented control, which involves directly orienting the current vectors with their corresponding controllers [8]. The second mode is indirect field-oriented control, which includes additional torque and flux control loops to indirectly regulate the current vectors [9]. Direct torque control (DTC) also is a classical method used in AC drives, including Syn-RM, that offers advantages over FOC in terms of response time [10, 11]. DTC enables quick responses to changes in speed and load, making it a preferred approach for torque and flux control [12]. However, the major disadvantage of this approach is the occurrence of high ripples in both flux and electromagnetic torque [13-16]. To overcome the shortcomings of traditional classical methods, the advanced control technique of model predictive control (MPC) has been utilized to drive the Syn-RM machine. MPC approach has gained popularity among researchers for its straightforward design, remarkable dynamic performance, and ease of application [17-22].

The MPC approach has the ability to predict the controlled variables, such as current, torque, and flux, in the subsequent time step before implementing the corresponding control actions. In literature, model

[1] Laboratoire de Modélisation des Systèmes Énergétiques, LMSE. University of Biskra, Biskra, Algeria
[2] Department of Electrical Engineering, LI3CUB Laboratory, University of Biskra, Biskra, Algeria
[3] Department of Electronics, Faculty of Technology, Contantine 1 University, Constantine, Algeria
[4] CISE – Electromechatronic Systems Research Centre, University of Beira Interior, Covilhã, Portugal
[5] Laboratoire de Génie Energétique et Matériaux, LGEM, University of Biskra, Biskra, Algeria
mohamedessalih.boussouar@univ-biskra.dz

https://doi.org/10.2478/jee-2023-0042, Print (till 2015) ISSN 1335-3632, On-line ISSN 1339-309X

predictive control (MPC) can be found in two sub-methods, namely, model predictive current control (MPCC) and model predictive torque control (MPTC). In [23], a new method called Direct Predictive Control (DPC) was introduced, which minimizes the current ripple by selecting the optimal voltage vectors in a hierarchical manner. Although MPCC exhibits exceptional performance in Syn-RM drives, its effectiveness heavily relies on the precise knowledge of the system model and its parameters, which may vary during operation due to magnetic saturation, iron losses, and temperature fluctuations [24]. As a result, conventional MPCC may not be effective in real applications.

Various scientific studies have been conducted to address the challenges mentioned earlier. A considerable amount of attention has been dedicated to the development of a model-free MPCC for PMSM [25-27]. However, only a limited number of studies have focused on Syn-RM. In [24], a model-free PCC based on Extended State Observer (ESO) was used to estimate the nonlinear unknown dynamics that need to be included in PMSM control. The authors in [28] proposed a model-free PCC based on a recurrent neural network (RNN) for Syn-RM. This approach allows compensation of the motor parametric variations by updating the weights of the RNN. In [29], the current difference detection technique (CDDT) is utilized in conjunction with PCC to mitigate the impact of parameter changes in Syn-RM. Another model-free PCC approach was presented in [30], which relied on reconstructing the predicted currents from previously stored measurements. The disturbance observation methods have also proved their effectiveness to compensate for the unknown dynamic changes caused by the parameter variations, as presented in [31, 32].

Time-delay estimation (TDE) is an effective technique employed to estimate uncertain and complex dynamics in the control system. Overall, the TDE-based model-free control method can provide significant advantages over other model-free control methods, including improved robustness, flexibility to be applied to a wide range of systems, reduced tuning effort, less implementation complexity, and improved performance. This paper presents a model-free control scheme designed to address unknown dynamics and parameter variations in the Syn-RM system, including inductances and stator resistor, using only inputoutput data measurements. Here, the current dynamic functions and their related parameters are initially considered unknown. To address this, ultra-local models are employed, as proposed in [33], and the local functions are approximated using the TDE technique. This approach allows the proposed TDE-based model-free predictive current control (TDE-MFPCC) to eliminate the need for prior knowledge of a precise current model and the identification of parameter values. Thus, the proposed controller offers an alternative method of control that requires minimal computation and is easily implemented in real-time. Furthermore, the control parameters are automatically selected using a metaheuristic optimization algorithm to achieve the best performance of the Syn-RM system.

The rest of this paper is organized as follows. In Section 2, the mathematical model of the Syn-RM used in developing the proposed control strategy is presented. Section 3, describes the controller design process of the conventional model-based current predictive control method. The robust model-free current predictive control law based on the time-delay estimation technique and PSO algorithm is discussed in Section 4. The numerical results to demonstrate the effectiveness of the proposed control strategy are shown and discussed in Section 5. Finally, the conclusions of this paper and some directions for future works are given in Section 6.

2 Dynamic model of Syn-RM

The structure of a Syn-RM consists of a stator with a set of windings and a rotor with a set of salient poles. The stator winding is energized with a three-phase AC supply, which produces a rotating magnetic field that interacts with the rotor saliency. As the magnetic field rotates, the rotor poles are magnetically attracted to the nearest stator pole, resulting in torque production. To keep the control system simple, the electrical model of Syn-RM is represented in the d,q reference frame of the rotor, expressed as:

$$\begin{cases} \dot{\psi}_d = -R_s I_d + \omega_e L_q I_q + V_d \\ \dot{\psi}_q = -R_s I_q - \omega_e L_d I_d + V_q \end{cases} \quad (1)$$

where V_d and V_q represent the d,q control voltages applied to the Syn-RM, I_d and I_q are the corresponding currents, w_e is the electrical angular speed, L_d and L_q stand for d,q inductances, R_s denotes the stator resistor. ψ_d and ψ_q are the flux links approximated by the expressions:

$$\begin{cases} \dot{\psi}_d = L_d I_d \\ \dot{\psi}_q = L_q I_q \end{cases} \quad (2)$$

The mechanical speed dynamic is given by:

$$\dot{w}_m = \frac{1}{j}(T_e - B_m w_m - T_L) \quad (3)$$

where T_e is the resulting electromagnetic torque stated in (4), j and B_m are the friction coefficient and moment of inertia, respectively, and T_L is the load torque, with p denoting the pole pairs number.

$$T_e = \frac{3}{2} P\big(L_d - L_q\big) I_d I_q \quad (4)$$

The electrical dynamic model of the Syn-RM motor in the d,q reference frame can be described by the following equations:

$$\begin{cases} \dot{I}_d = \dfrac{1}{L_d}\left(-RsI_d + pw_m L_q I_q + V_d\right) \\ \dot{I}_q = \dfrac{1}{L_q}\left(-RsI_q - pw_m L_d I_d + V_q\right) \end{cases} \quad (5)$$

Figure 1 shows a general structure of the Syn-RM rotor, whilst Fig. 2 illustrates the Syn-RM coordinates. The d and q axis are presented with respect to stator reference frame α and β.

From the dynamic model equations (1) to (4), it is clearly noted that the Syn-RM system is a nonlinear system whose internal parameters are mostly unknown and cannot be measured in real-time, such as the electrical parameters R_s, L_d, and L_q. The load torque T_L in (3) is regarded as an unknown external disturbance whose values are dependent on the operating conditions. The challenge of Syn-RM control is to ensure stable performance throughout the whole operation region taking into account any eventual system characteristic variation.

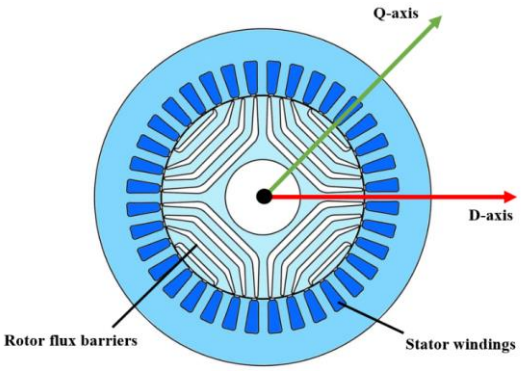

Fig. 1. Syn-RM rotor structure

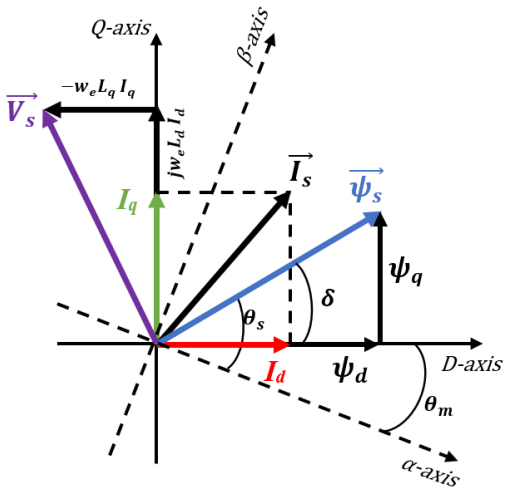

Fig. 2. Syn-RM coordinates

3 Conventional model-based current predictive control

The conventional MB-PCC investigated in this section consists of two control loops, an outer loop for speed control and an inner loop for current predictive control. The main purpose of this paper is to address the current control problem, whereas the control of the Syn-RM speed is carried out using a classical proportional-integral (PI) controller, As depicted in Fig.3, the value of current reference $I^*_{q|k}$ is obtained from the speed control loop, and $I^*_{d|k}$ is calculated based on maximum torque per ampere (MTPA) control [28]. The current control is performed via a model-based predictive controller that uses system parameters to predict current using Euler's approximation. The discrete form of the currents predicted in (5) can be written as:

$$\begin{cases} I_{d|k+1} = \left(1 - \dfrac{R_s T_s}{L_d}\right) I_{d|k} + \omega_e T_s \dfrac{L_q}{L_d} I_{q|k} + \dfrac{T_s}{L_d} V_{d|k} \\ I_{q|k+1} = \left(1 - \dfrac{R_s T_s}{L_q}\right) I_{q|k} - \omega_e T_s \dfrac{L_d}{L_q} I_{d|k} + \dfrac{T_s}{L_q} V_{q|k} \end{cases} \quad (6)$$

where $I_{d|k}$ and $I_{q|k}$ are the measured currents at the k^{th} time step, T_s is the sampling time, and $V_{d|k}$ and $V_{q|k}$ are the applied voltage components.

The selected voltage vectors are optimized through a short iteration algorithm containing the eight possible voltage vectors candidates, the cost function equation below (6) minimizes the errors between the reference currents and their predicted values [34]

$$g = \left[I^*_{d|k} - I_{d|k+1}\right]^2 + \left[I^*_{q|k} - I_{q|k+1}\right]^2 + I_{sat}\,, \quad (7)$$

where
I_{sat} is a protection constraint value related to the predicted current $i_{s|k+1}$ defined as:

$$I_{sat} = \begin{cases} \infty, & \text{if } \left|I_{s|k+1}\right| > \left|I_{s_{max}}\right| \\ 0, & \text{otherwise.} \end{cases},$$

$$\left|I_{s|k+1}\right| = \sqrt{I^2_{d|k+1} + I^2_{q|k+1}}\,. \quad (8)$$

The model-based MPC can provide good performance and precise control. However, its dependence on machine dynamics made this control

structure less robust and difficult to implement, especially the variation of motor inductances caused by magnetic saturation

***Remark 1*:** In most AC drive control schemes, speed control is usually performed using classical PI due to the slow dynamics of the mechanical speed and it is less affected by parameter changes. In Fig. 3 the speed error is minimized with a simple PI control, and parameters K_P and K_I are given in Table 3.

4 Proposed model-free current predictive control

In this section, a control scheme is suggested that combines the PCC approach with model-free control, as proposed by Fliss and Joint in [33]. The scheme is made more robust through the use of the TDE technique, which estimates local unknown dynamics and uncertainties. Hence, the nonlinear dynamics of the currents in equation (6) are represented by ultra-local models. To estimate the local dynamics, the TDE approach is utilized, and the Particle Swarm Optimization (PSO) algorithm is employed to optimize the design parameters. The overall control scheme of the proposed method is depicted in Fig. 3.

4.1 Ultra local model

For a given non-linear dynamic system, its general ultra-local expression can be written as,

$$y^v = f(t) + \alpha U, \tag{9}$$

where

y^v is the v^{th} derivative of the system output y,
$f(t)$ is the lumped uncertainties resulting from unmodeled dynamics, and unknown disturbances,
U is the control input signal,
α is a given constant.

The complex dynamic model of Syn-RM in (1) can be represented by an ultra-local model according to (9) as follows:

$$\begin{cases} \dot{I}_d = f_d(t) + \alpha_d V_d \\ \dot{I}_q = f_q(t) + \alpha_q V_q \end{cases} \tag{10}$$

where f_d and f_q are the lumped parameter uncertainties and nonlinear dynamic functions which are considered unknowns, α_d and α_q are design constants. In model-free control design, various techniques were proposed to estimate the unknown dynamic functions such as extended state observer approach [24], nonlinear disturbance compensation technique [25], adaptive neural network approximator based on extended Kalman filter [28]. In this study, the TDE technique is proposed to estimate all the unknown dynamic functions and parameter variations. This approach is easy to implement since it only requires the measured input/output data of the system to compute the unknown functions with a small computational burden.

4.2 TDE-based model-free control

The estimation accuracy of f_d and f_q can have an impact on control performance since it includes the dynamics or disturbances of the system. As a result, the solution of f_i for $i \in \{d, q\}$ becomes a key problem for this approach. TDE is frequently utilized to estimate unknown nonlinear dynamics, where time-delayed signals are used to estimate the lumped uncertainty and bring about a simple and useful model-free feature [35]. Consequently, using the TDE approach, an acceptable approximation of f can be obtained; $f_i(t-\varepsilon)$ is regarded as the estimated value of $f_i(t)$. As long as the time delay is minimal, it is considered $\hat{f}_i(t) \approx f_i(t) \approx f_i(t-\varepsilon)$, and thus:

$$\hat{f}_i(t) = \dot{y}_i(t) - \alpha U_i(t) \tag{11}$$

$$\hat{f}_i(t) \approx \hat{f}_i(t-\varepsilon) = \dot{y}_i(t-\varepsilon) - \alpha U_i(t-\varepsilon) \tag{12}$$

To achieve a stable control output and prevent excessive chattering, a low pass filter (LPS) is introduced in the calculation of $\hat{f}_i(t)$. Additionally, fast converging gains β_d and β_q have been incorporated into the proposed TDE to expedite the convergence of the control algorithm. The values of $\hat{f}_d$ and $\hat{f}_q$ are thus estimated using the following formulas:

$$\begin{cases} \hat{f}_d(t) = \beta_d\left[\mathrm{LPS}\left[\dot{I}_d(t-\varepsilon) - \alpha_d V_d(t-\varepsilon)\right]\right] \\ \hat{f}_q(t) = \beta_q\left[\mathrm{LPS}\left[\dot{I}_q(t-\varepsilon) - \alpha_q V_q(t-\varepsilon)\right]\right] \end{cases} \tag{13}$$

First-order LPS is adopted, with the transfer function given as follows:

$$\begin{cases} h_d(P) = \dfrac{1}{\dfrac{1}{w_d}P + 1} \\ h_q(P) = \dfrac{1}{\dfrac{1}{w_q}P + 1} \end{cases} \tag{14}$$

where w_d and w_q are the cut-off frequencies to be optimized, the coefficients $\alpha_{d,q}$ are selected close to the reversed rated inductances d, q respectively, that are

$$\alpha_d = \frac{1}{L_d} \text{ and } \alpha_q = \frac{1}{L_q}.$$

The discrete version of (10) can be obtained using Euler approximation as follows:

$$\begin{cases} I_{d|k+1} = \hat{f}_{d|k} T_s + \alpha_d V_{d|k} T_s + I_{d|k} \\ I_{q|k+1} = \hat{f}_{q|k} T_s + \alpha_q V_{q|k} T_s + I_{q|k} \end{cases} \quad (15)$$

where $I_{d,q|k}$ and $V_{d,q|k}$ are the d, q currents and input voltage respectively, T_s stands for the sampling time.

Assumption 1: The estimated values of $\hat{f}_d(t)$ and $\hat{f}_q(t)$ are considered bounded such that $|\hat{f}_d(t)| \leq \Delta_d$ and $|\hat{f}_q(t)| \leq \Delta_q$, where Δ_d and Δ_q are the upper boundaries of $\hat{f}_d(t)$ and $\hat{f}_q(t)$, respectively.

***Remark 2*:** The inclusion of derivative terms in TDE equations has led to high fluctuations in the estimated values of $\hat{f}_d$ and $\hat{f}_q$, as shown in equation (13). In order to address this issue, a Low Pass Filter (LPS) has been incorporated in the TDE output to reduce the ripple effect.

4.3 Optimization of the TDE-MFPCC using particle swarm algorithm (PSO)

In the proposed control scheme, the coefficients $\beta_{d,q}$ and LPS cut-off frequencies $w_{d,q}$ are optimized with PSO algorithm, which is a computational technique for optimizing a particular problem by iteratively attempting to improve a candidate solution in relation to a specified quality measure. In the process of PSO, it begins by selecting a random set of unknown parameter values, with each set representing a particle swarm, the goal function corresponding to each particle is computed using each position and velocity of the current particle, Then, the particle whose objective value matches to the optimal value is picked and recorded after each iteration of the algorithm, and ultimately the global best solution is generated [35], The PSO process flowchart is depicted in Fig. 4.

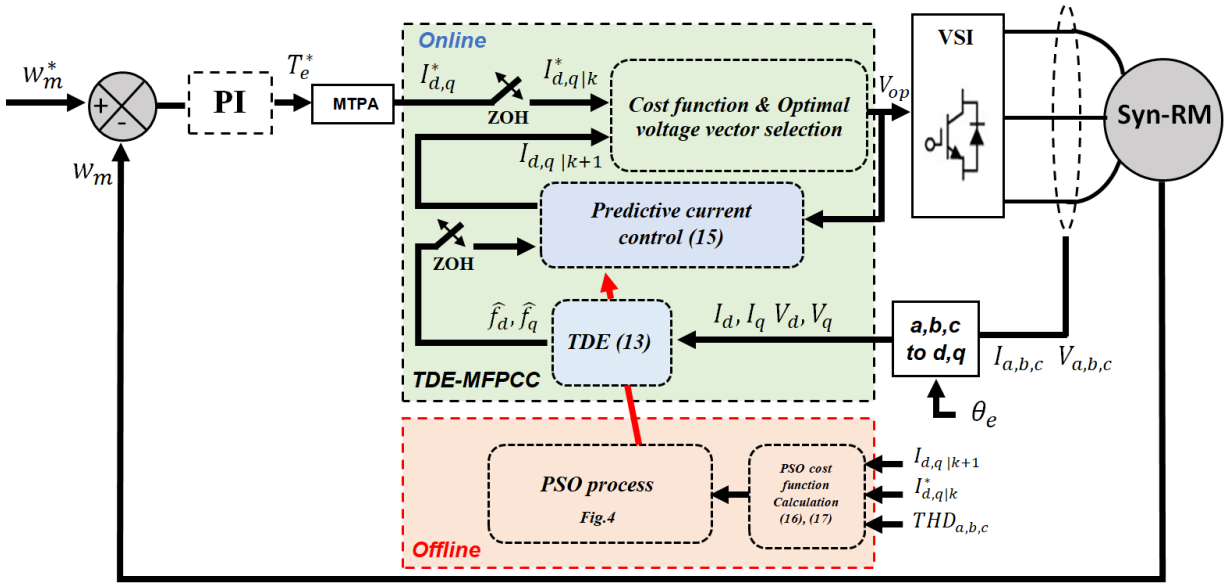

Fig. 3. Proposed TDE-MFPCC block diagram

$\beta_{d,q}$ used in (13) is defined through the PSO algorithm process based on the minimization of the cost function G_β :

$$\begin{cases} Find\ X = (\beta_d, \beta_q) \\ G_\beta = \text{ To minimize }_{obj}(X) = \\ = min\left[\left(I_{d|k}^* - I_{d|k+1}\right) + \left(I_{d|k}^* - I_{d|k+1}\right)\right] \end{cases} \quad (16)$$

The total harmonic distortion (THD) of the three-phase currents (a, b, c) measurement is minimized to achieve optimal settings $w_{d,q}$ according to the cost function G_w defined as:

$$\begin{cases} Find\ X = (w_d, w_q) \\ G_w = \text{ To minimize }_{obj}(X) = \\ = min[THD_a + THD_b + THD_b] \end{cases} \quad (17)$$

The swarm particle velocity $vi(t\ +\ 1)$ is updated using the last best global solution p_g as stated in the following:

$$v_i(t+1) = wv_i(t) + c_1 r_1 \left(p_i - x_i(t)\right) + \\ + c_2 r_2 \left(p_g - x_i(t)\right) \quad (18)$$

where w is the inertia weight, c_1 and c_2 represent the cognition learning and the social learning factors, respectively, and $r_1, r_2 \in [0,1]$ are generated random

numbers, p_g is the current best global position, whilst p_i denotes the local best position of the current PSO iteration. The new position is then updated as follows:

$$x_i(t+1) = x_i(t) + v_i(t+1). \quad (19)$$

The pseudo-code written in Algorithm.1 represents a brief description of the PSO process used for parameters optimization through 100 iterations of 10 swarm particle candidates.

***Remark 3*:** There are many optimization techniques in the literature to achieve an optimum solution for a given problem. This paper chooses a PSO algorithm to find the best control parameters due to its favorable characteristics and suitability in such optimization issues.

Algorithm 1: Pseudo-code of the PSO algorithm

Cost function $\mathbf{G_n}$ for $\mathbf{n} \in \{\boldsymbol{\beta_d}, \boldsymbol{\beta_q}, \boldsymbol{w_d}, \boldsymbol{w_q}\}$
Swarm initialization: the position $\boldsymbol{x_i(t)}$ and velocity $\boldsymbol{v_i(t)}$ are initialized randomly
for $\boldsymbol{t} \leftarrow \mathbf{1}$ to 100 (Iteration number)
for $\boldsymbol{i} \leftarrow \mathbf{1}$ to 10 (Swarm size)
Evaluate and update the local best $\boldsymbol{G_n(p_i(t))}$ based on the result of (16) and (17)
if $\boldsymbol{G_n(x_i(t)) < G_n(p_i(t))}$ then
update the best position $\boldsymbol{p_i(t)}$, that is $\boldsymbol{p_i(t) = x_i(t)}$
end if
end for
$\boldsymbol{G_n(p_g(t)) = \min_i(G_n(p_i(t)))}$
Evaluate and update the global best $\boldsymbol{G_n(p_g(t))}$ after each swarm iteration update particle velocity $\boldsymbol{v_i(t+1)}$ using (18)
update particle position $\boldsymbol{x_i(t+1)}$ using (19)
end for
Rank the solutions and find the global best of $\boldsymbol{\beta_{d,q}}$ and $\boldsymbol{w_{d,q}}$.

Table 1. Syn-RM parameters

Parametre	Value
Rated power	2.2 kW
Rated current	5.7 A
Rated speed	1500 rpm
Rated Torque	14 N.m
N^o of pole pairs	2
Moment of inertia (J)	0.0137 kg.m/s
Stator resistance	1.71 Ω

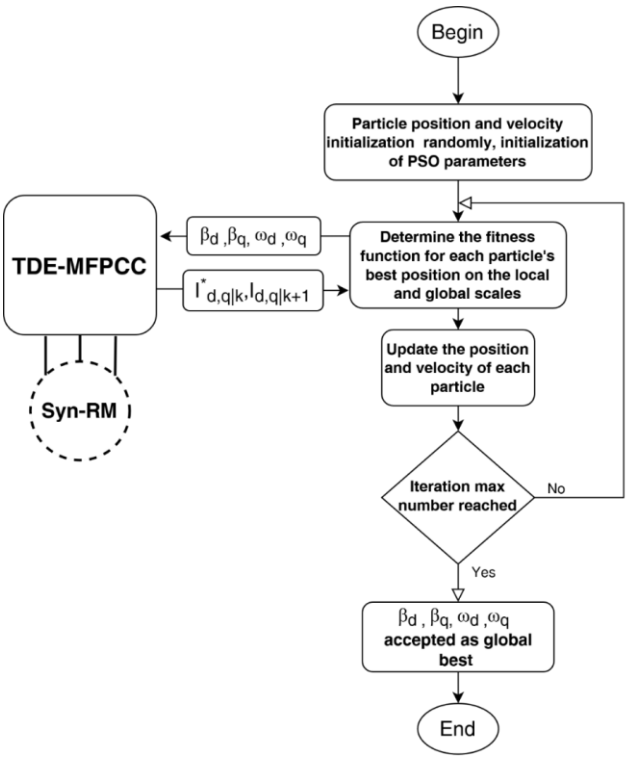

Fig. 4. Flowchart of particle swarm optimization algorithm

5 Simulation and discussion

The simulation of the proposed control was conducted in MATLAB/Simulink, where a non-linear model of Syn-RM was implemented in the overall scheme, with nominal parameters presented in Table. I. The sample time is set to 0.00005 s as well as the delay time used in TDE estimation equation (13). For a fair comparison between the proposed method and the conventional MB-PCC, the same PI speed controller parameters were tuned for both strategies, in order to simulate the effect of parameters mismatch on Syn-RM PCC control both L_d and L_q are set to 50 % of their rated values. The results of the last iteration of PSO process are presented in Fig. 15 and Fig. 16 in appendix for $\beta_{d,q}$ and $w_{d,q}$ employed in (13), (14) respectively, containing the local best value of each swarm (small blue stars) and the globally optimal solution (big orange stars).

5.1 Load change burden

Figure 5 shows the simulation results of the conventional MB-PCC and the proposed TDE-MFPCC approach for the same test run scenario under identical initial operating conditions. Initially, a load of 10 Nm was applied and the speed reference is set to 1500 rpm (rated value). Subsequently, at t=2 s, the load was incrementally increased to the rated value of 14 Nm. Figure 5(a) depicts the outcomes of MB-PCC with precise motor parameters. The speed response is showcased in the first channel, while the second channel

displays the phase (A) current. The third channel exhibits the obtained response of $I_{d,q}$ as well as their references $I^*_{d,q}$. It is clear that the effectiveness of MB-PCC's performance becomes evident when accurate motor parameters are taken into account in the control process. Fig. 5(b) depicts the responses obtained using MB-PCC with mismatched model parameters, where increased current THD. It is clear that the current response deviates more from the target signal when the load increases. The results of the suggested TDE-MFPCC are depicted in Fig. 5(c). In contrast to the MB-PCC, the proposed control scheme has better steady-state performance and less THD. The lumped uncertainties estimate $\widehat{f_d}$ and $\widehat{f_q}$ response is shown in Fig.13, where steady-state performance is achieved owing to the system dynamic behavior reflected by the TDE technique.

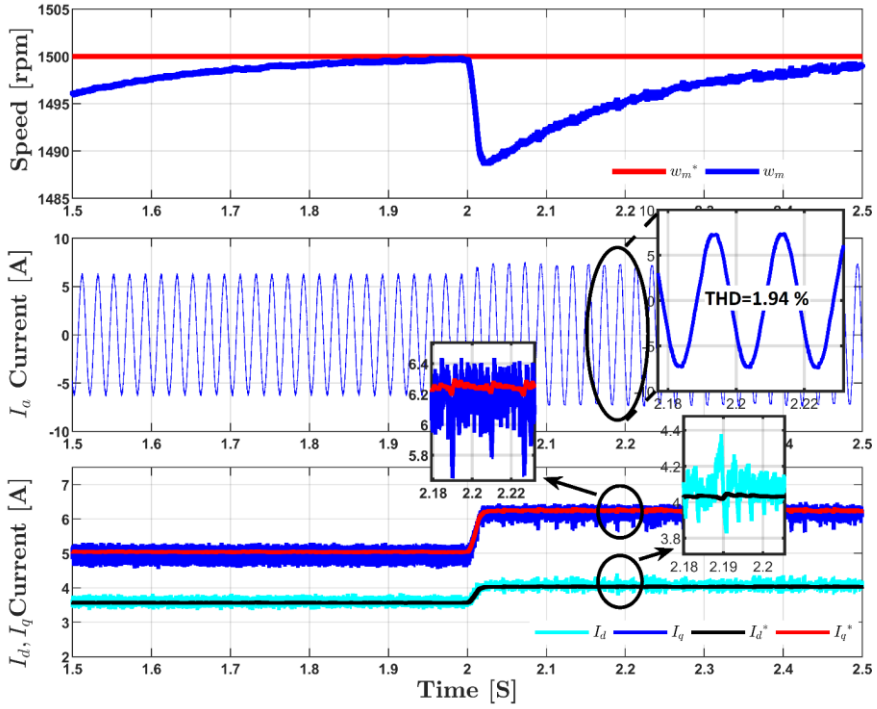

(a)

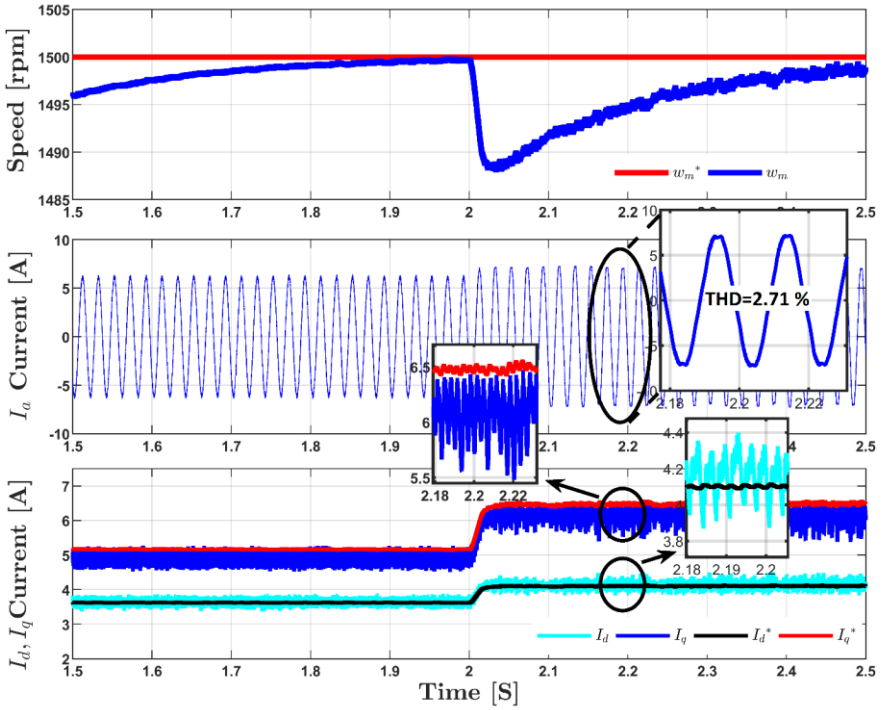

(b)

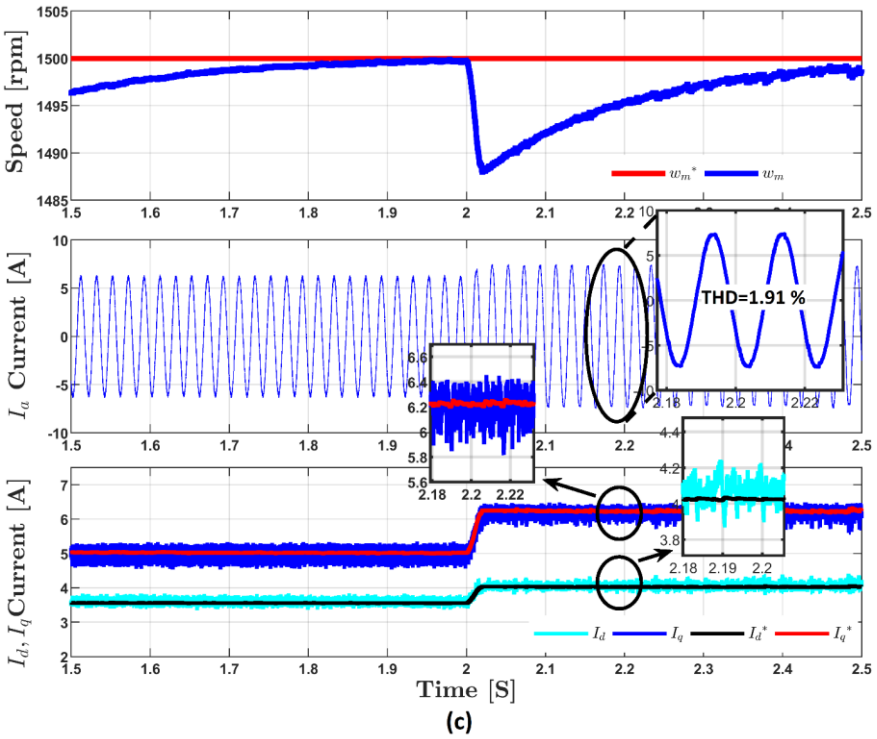

Fig. 5. Simulation results under a load change: (a) conventional MB-PCC with accurate parameters; (b) conventional MB-PCC with mismatched parameters; (c) proposed TDE-MFPCC

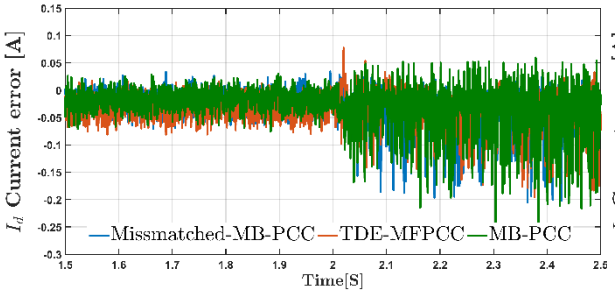

Fig. 6. I_d current tracking error under load change

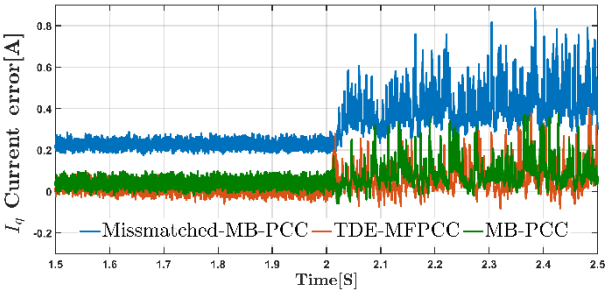

Fig. 7. I_q current tracking error under load change

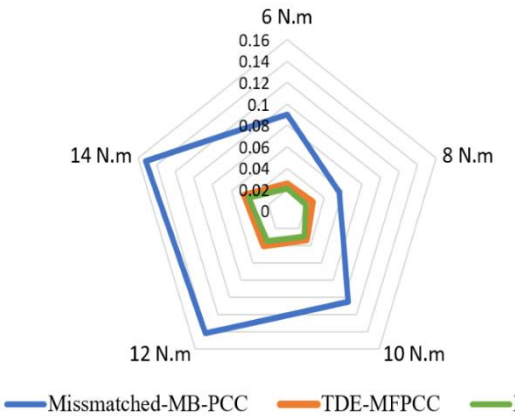

Fig. 8. I_d current tracking error in function of load torque

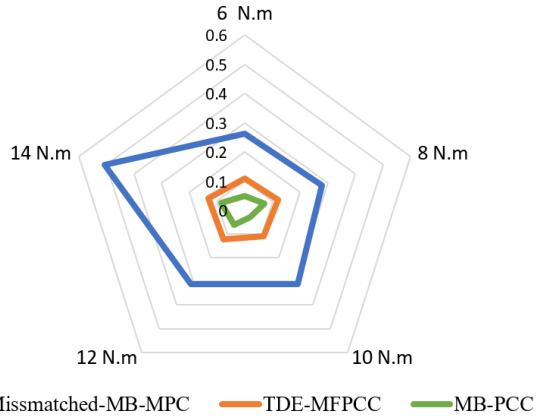

Fig. 9. I_q current tracking error in function of load torque

Figures 6 and 7 depict the current tracking errors for I_d and I_q of the presented control schemes when the Syn-RM is under the effect of load torque. It is clear also that the parameter mismatch has a significant effect on the current control. Besides, in the MB-PCC with accurate parameters and the proposed TDE-MFPCC, the tracking errors were reduced significantly in the load change case. To further highlight the robustness of the proposed control scheme compared to the other control approaches, the chart of tracking errors of I_d and I_q according to the multivariate load torque have been also shown in Fig. 8 and Fig. 9. It can be seen that when using MB-PCC with mismatched parameters, the I_q error increases proportionally with load variation. Whereas, the proposed TDE-MFPCC reduces the gap between the current reference and its actual value similar to MB-PCC with accurate parameters.

5.2 Speed variation burden

Figure 10 depicts the simulation results of the aforementioned control methods, where a speed variation test was conducted. The initial load was set to 10 Nm, and the speed was set to 800 rpm. Subsequently, at t=1.8 s, the speed was incremented to its rated value of 1500 rpm. The obtained results in Fig. 10 (b) indicate that the parameter mismatch has also a considerable effect on conventional MB-PCC in speed variation cases. The third channel of Fig. 10 (b) shows the I_q current error that increases significantly with the speed variation, while the TDE-MFPCC was less affected by speed change, see Fig. 11 and Fig. 12. Considering the values of THD, the current distortion has been reduced thanks to the disturbance compensation function provided by the TDE technique. In Fig. 10 (b), the MB-PCC Phase (A) response shows the effect of inaccurate parameters which led to a high THD value compared to the TDE-MFPCC. Phase (A) THD has a lower value compared to the MB-PCC with exact parameters as depicted in Fig. 10 (a). For further analysis of the proposed TDE-MFPCC method, the lumped uncertainties estimated $\widehat{f_d}$ and $\widehat{f_q}$ are illustrated in Fig. 14. Here, one can conclude that the evolution of the unknown current dynamics is well compensated during the speed variation test using TDE formulation. Also, it is seen that the parameter mismatch has a significant effect on the current control when the speed increases. Unlike, the MB-PCC with accurate parameters has less current deviation. To sum up, the obtained result within the simulation tests compared issues of the three presented schemes MB-PCC and TDE-MFPCC were illustrated in Table 2.

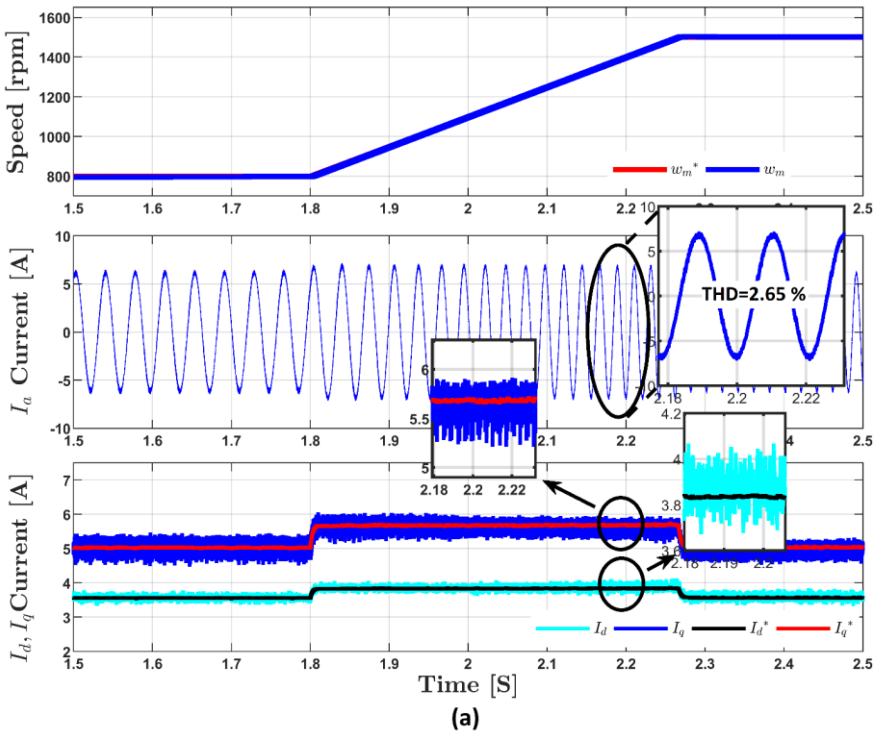

(a)

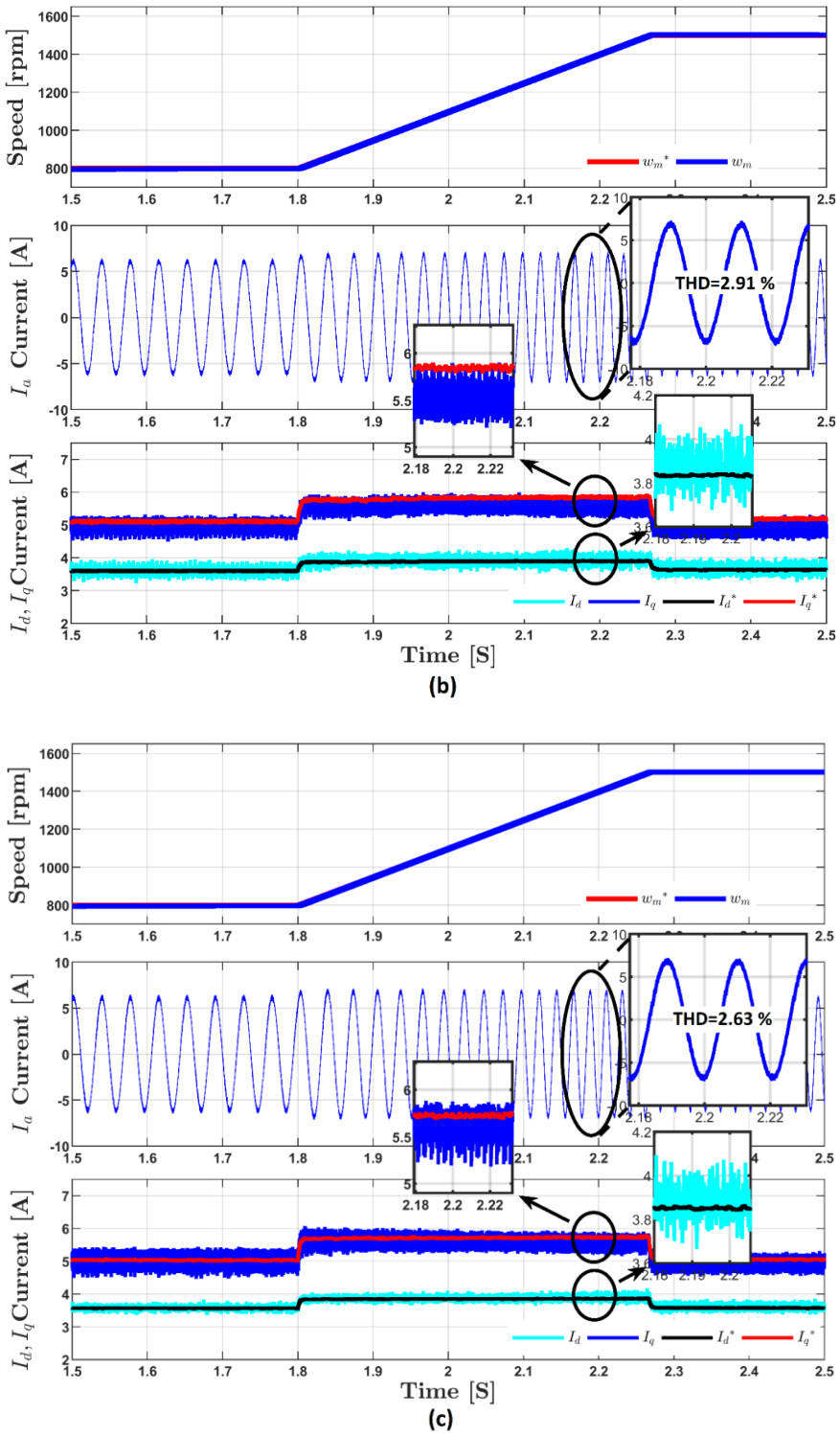

Fig. 10. Simulation results under speed change: (a) conventional MB-PCC with accurate parameters, (b) conventional MB-PCC with mismatched parameters, (c) proposed TDE-MFPCC

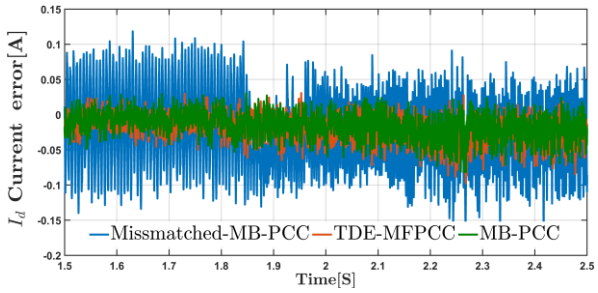

Fig. 11. I_d current tracking error under speed variation

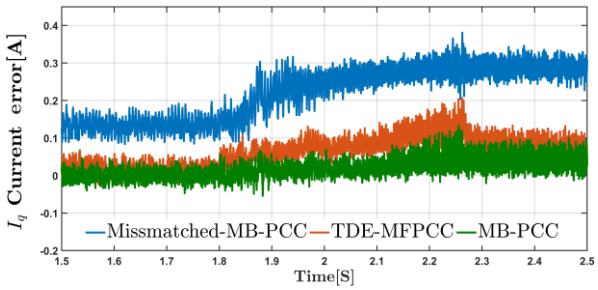

Fig. 12. I_q current tracking error under speed variation

Table 2. Comparative issues

Syn-RM PCC scheme	Computation time	Motor parameters needed	Algorithm complexity	Tuned parameters
Conventional MB-PCC	27.5 μs	R_s, L_d, L_q	Low	Null
Proposed TDE-MFPCC	26.0 μs	Null	Low	$\beta_{d,q}, w_{d,q}$

6 Conclusions

In this paper, a new optimal model-free predictive control approach for Syn-RM drive based on a time-delay estimation (TDE) technique has been proposed. By combining the model-free control theory and the TDE approximator, this proposed control system is able to deal with uncertainties and disturbance problems and allows it to give a robust and straightforward control scheme that can be implemented in real-time applications. By introducing a particle swarm optimization (PSO) metaheuristic algorithm, the control design parameters were optimized to improve the electrical dynamic performances of the Syn-RM system. To give more simplicity, the speed control is implemented by the conventional proportional-integral controller in the outer loop, whereas the proposed TDE-based model-free predictive current control (TDE-MFPCC) is employed in the inner loop to effectively stabilize the internal dynamics of the Syn-RM machine. Extensive numerical results have been presented to illustrate the best performance of the proposed control algorithm in comparison with the conventional model-based predictive controller. In the future, the proposed controller will be tested on a real device dealing with the limits of the control saturation and using robust observers to estimate the system states.

Table 3. Simulation settings

Parameters	Value
Proportional gain K_P	0.2
Integral gain K_I	0.8
D-axis inductance L_d	0.26 H
Q-axis Inductance L_q	0.057 H
α_d	4.1
α_q	17.5
β_d	2.6
β_q	22.1
ω_d	167.3 rad/s
ω_q	153.8 rad/s
PSO swarm set number	10
PSO iteration number	100
Sampling time T_s	50 μs

Appendix

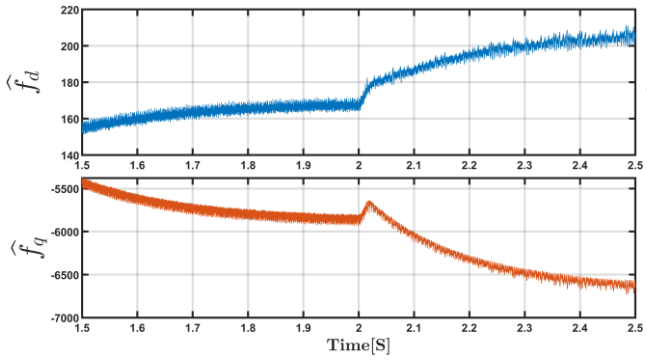

Fig. 13. Estimated lumped uncertainties $\hat{f}_d$ and $\hat{f}_q$ in load change case

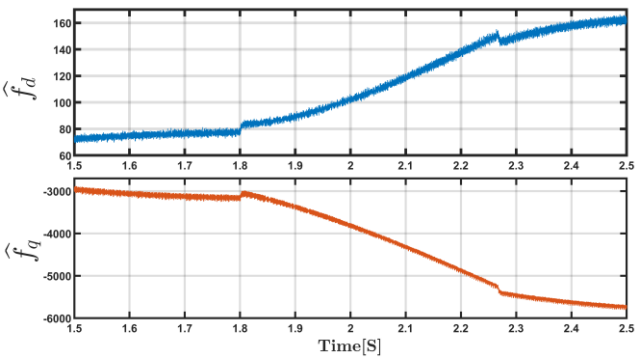

Fig. 14. Estimated lumped uncertainties $\hat{f}_d$ and $\hat{f}_q$ in speed change case

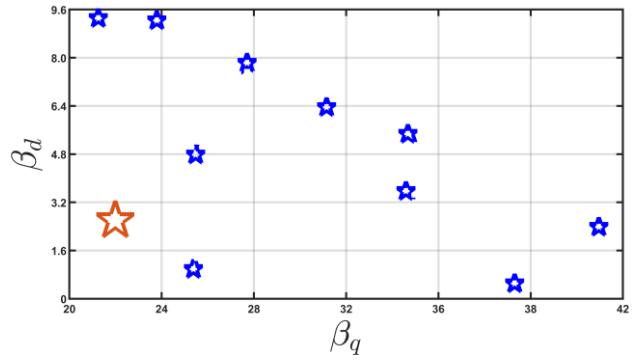

Fig. 15. Last iteration of PSO swarms in the process of $\beta_{d,q}$ optimization

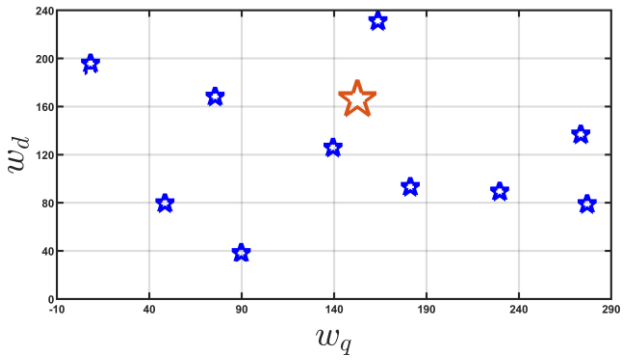

Fig. 16. Last iteration of PSO swarms in the process of $\omega_{d,q}$ optimization

References

[1] T. Hamiti, T. Lubin, L. Baghli, and A. Rezzoug, "Modeling of a synchronous reluctance machine accounting for space harmonics in view of torque ripple minimization," *Mathematics and Computers in Simulation*, vol. 81, no. 2, pp. 354-366, 2010.

[2] G. H. B. Foo and X. Zhang, "Robust direct torque control of synchronous reluctance motor drives in the field-weakening region," *IEEE Transactions on Power Electronics*, vol. 32, no. 2, pp. 1289-1298, 2017.

[3] H. Hadla and S. Cruz, "Predictive stator flux and load angle control of synchronous reluctance motor drives operating in a wide speed range," *IEEE Transactions on Industrial Electronics*, vol. 64, no. 9, pp. 6950-6959, 2017.

[4] S. E. Lyshevski, "Nonlinear modeling and robust control of synchronous reluctance motors," *Energy Conversion and Management*, vol. 43, no. 4, pp. 523-536, 2002.

[5] D. Igrec, A. Chowdhury, B. Štumberger, and A. Sarjaš, "Robust tracking system design for a synchronous reluctance motor – SynRM based on a new modified bat optimization algorithm," *Applied Soft Computing*, vol. 69, pp. 568-584, 2018.

[6] L. Xu, X. Xu, T. Lipo, and D. Novotny, "Vector control of a synchronous reluctance motor including saturation and iron loss," *IEEE Transactions on Industry Applications*, vol. 27, no. 5, pp. 977-985, 1991.

[7] T. Matsuo and T. Lipo, "Field oriented control of synchronous reluctance machine," in *Proceedings of IEEE Power Electronics Specialist Conference - PESC '93*, pp. 425-431, 1993.

[8] H. Hadla and F. Santos, "Performance comparison of field-oriented control, direct torque control, and model-predictive control for SynRMs," *Chinese Journal of Electrical Engineering*, vol. 8, no. 1, pp. 24-37, 2022.

[9] C. Li, Q. Du, and X. Liu, "Indirect predictive torque control for switched reluctance motor in ev application," Energy Reports, vol. 8, pp. 857-865, 2022.

[10] X. Zhang and G. H. B. Foo, "A robust field-weakening algorithm based on duty ratio regulation for direct torque controlled synchronous reluctance motor," *IEEE/ASME Transactions on Mechatronics*, vol. 21, no. 2, pp. 765-773, 2016.

[11] R. Morales-Caporal and M. Pacas, "Encoderless predictive direct torque control for synchronous reluctance machines at very low and zero speed," *IEEE Transactions on Industrial Electronics,* vol. 55, no. 12, pp. 4408-4416, 2008.

[12] M. Rosic, B. Koprivica, and M. Bjekic, "Smart DTC algorithm with automatic torque ripple adjustment," *Journal of Electrical Engineering*, vol. 73, no. 2, pp. 88-98, 2022.

[13] Y.-S. Choi, H. H. Choi, and J.-W. Jung, "Feedback linearization direct torque control with reduced torque and flux ripples for IPMSM drives," *IEEE Transactions on Power Electronics*, vol. 31, no. 5, pp. 3728-3737, 2016.

[14] P. H. Truong, D. Flieller, N. K. Nguyen, J. Mercklé, and G. Sturtzer, "Torque ripple minimization in non-sinusoidal synchronous reluctance motors based on artificial neural networks," *Electric Power Systems Research*, vol. 140, pp. 37-45, 2016.

[15] P. R. Ghosh, A. Das, and G. Bhuvaneswari, "Comparative analysis of sensorless DTC schemes for a synchronous reluctance motor drive," in 2018 *IEEE International Conference on Power Electronics, Drives and Energy Systems (PEDES)*, pp. 1-5, 2018.

[16] T. A. Huynh, N.-D. Le, M.-F. Hsieh, and D.-K. Ngo, "A modified of DTC control applied to novel FI-PMA-SynRM for torque ripple reduction," in *2019 IEEE 4th International Future Energy Electronics Conference (IFEEC)*, pp. 1-7, 2019.

[17] I. Hammoud, S. Hentzelt, T. Oehlschlaegel, and R. Kennel, "Learning-based model predictive current control for synchronous machines: An LSTM approach," *European Journal of Control*, vol. 68, p. 100663, 2022. 2022 European Control Conference Special Issue.

[18] F. Morel, X. Lin-Shi, J.-M. Rétif, and B. Allard, "A predictive current control applied to a permanent magnet synchronous machine, comparison with a classical direct torque control," *Electric Power Systems Research*, vol. 78, no. 8, pp. 1437-1447, 2008.

[19] T. Li, X. Sun, G. Lei, Y. Guo, Z. Yang, and J. Zhu, "Finite-control-set model predictive control of permanent magnet synchronous motor drive systems – An overview," *IEEE/CAA Journal of Automatica Sinica*, vol. 9, no. 12, pp. 2087-2105, 2022.

[20] I. Hammoud, S. Hentzelt, K. Xu, T. Oehlschlägel, M. Abdelrahem, C. Hackl, and R. Kennel, "On continuous-set model predictive control of permanent magnet synchronous machines," *IEEE Transactions on Power Electronics*, vol. 37, no. 9, pp. 10360-10371, 2022.

[21] S. Chai, L. Wang, and E. Rogers, "Model predictive control of a permanent magnet synchronous motor with experimental validation," *Control Engineering Practice*, vol. 21, no. 11, pp. 1584-1593, 2013.

[22] C. Mai-Van, S. Duong-Minh, D. Tran-Huu, B. Binh-Pho, and P. Vu, "An improved method of model predictive current control for multilevel cascaded H-bridge inverters," *Journal of Electrical Engineering*, vol. 72, no. 1, pp. 1-11, 2021.

[23] R. Antonello, M. Carraro, L. Peretti, and M. Zigliotto, "Hierarchical scaled-states direct predictive control of synchronous reluctance motor drives," *IEEE Transactions on Industrial Electronics*, vol. 63, no. 8, pp. 5176-5185, 2016.

[24] Y. Zhang, J. Jin, and L. Huang, "Model-free predictive current control of PMSM drives based on extended state observer using ultralocal model," *IEEE Transactions on Industrial Electronics*, vol. 68, no. 2, pp. 993-1003, 2021.

[25] L. Xu, G. Chen, and Q. Li, "Ultra-local model-free predictive current control based on nonlinear disturbance compensation for permanent magnet synchronous motor," *IEEE Access*, vol. 8, pp. 127690-127699, 2020.

[26] S. Gao, Y. Wei, D. Zhang, H. Qi, Y. Wei, and Z. Yang, "Model-free hybrid parallel predictive speed control based on ultralocal model of PMSM for electric vehicles," *IEEE Transactions on Industrial Electronics*, vol. 69, no. 10, pp. 9739-9748, 2022.

[27] M. Lv, S. Gao, Y. Wei, D. Zhang, H. Qi, and Y. Wei, "Model-free parallel predictive torque control based on ultra-local model of permanent magnet synchronous machine," *Actuators*, vol. 11, no. 2, 2022.

[28] H. Mesai Ahmed, I. Jlassi, A. J. Marques Cardoso, and A. Bentaallah, "Model-free predictive current control of synchronous reluctance motors based on a recurrent neural network," *IEEE Transactions on Industrial Electronics*, vol. 69, no. 11, pp. 10984-10992, 2022.

[29] C.-K. Lin, T.-H. Liu, J.-t. Yu, L.-C. Fu, and C.-F. Hsiao, "Model-free predictive current control for interior permanent-magnet synchronous motor drives based on current difference detection technique," IEEE Transactions on Industrial Electronics, vol. 61, no. 2, pp. 667-681, 2014.

[30] P. G. Carlet, F. Tinazzi, S. Bolognani, and M. Zigliotto, "An effective model-free predictive current control for synchronous reluctance motor drives," *IEEE Transactions on Industry Applications*, vol. 55, no. 4, pp. 3781-3790, 2019.

[31] N. Yang, S. Zhang, X. Li, and X. Li, "A new model-free deadbeat predictive current control for PMSM using parameter-free Luenberger disturbance observer," *IEEE Journal of Emerging and Selected Topics in Power Electronics*, pp. 1-1, 2022.

[32] Y. Yu, Z. Mi, X. Zheng, D. Chang, X. Zheng, and C. Sun, "Adaptive sliding mode backstepping control-based maximum torque per ampere control of permanent magnet-assisted synchronous reluctance motor via nonlinear disturbance observer," *Advances in Mechanical Engineering*, vol. 10, no. 7, 2018, DOI: 10.1177/1687814018788750

[33] M. Fliess and C. Join, "Model-free control," *International Journal of Control*, vol. 86, no. 12, pp. 2228-2252, 2013.

[34] J. Riccio, P. Karamanakos, S. Odhano, M. Tang, M. D. Nardo, and P. Zanchetta, "Direct model predictive control of synchronous reluctance motor drives," *IEEE Transactions on Industry Applications*, pp. 1-10, 2022.

[35] G. I. Mustafa, H. Wang, and Y. Tian, "Vibration control of an active vehicle suspension systems using optimized model-free fuzzy logic controller based on time delay estimation," *Advances in Engineering Software*, vol. 127, pp. 141-149, 2019.

Received 17 May 2023